KEK-PREPRINT-92-37
Fermilab Library
0 1160 0009184 7

KEK Preprint 92-37
AMY 92-2
May 1992
H

A STUDY OF THE HADRON PRODUCTION IN $\gamma\gamma$ COLLISIONS WITH THE AMY DETECTOR

RYOTARO TANAKA

Department of Physics,
Chuo University
1-13-27 Kasuga, Bunkyoku, Tokyo 112, Japan

ABSTRACT

We presents results of an experimental study of $e^+e^- \rightarrow e^+e^- + hadrons$ with the no-tag condition. We observe more events than expected from the incoherent sum of QPM and VMD models and give a quantitative explanation of the excess by including the hard scattering effects of the hadronic constituents of the photons calculated with QCD.
Also presented are results of a measurement of the photon structure function F_2^γ at averaged Q^2 =51 (GeV/c)^2. The measured structure function is compared with the incoherent sum of the VMD and QCD predictions.

ROUTE TO
NAME
RETURN

Talk given at the IX International Workshop on Photon-Photon Collisions,
March 22-26, 1992, University of California, San Diego,
California, U.S.A.

National Laboratory for High Energy Physics, 1992

KEK Reports are available from:

Technical Information & Library
National Laboratory for High Energy Physics
1-1 Oho, Tsukuba-shi
Ibaraki-ken, 305
JAPAN

Phone:	0298-64-1171	
Telex:	3652-534	(Domestic)
	(0)3652-534	(International)
Fax:	0298-64-4604	
Cable:	KEKOHO	

A STUDY OF THE HADRON PRODUCTION IN $\gamma\gamma$ COLLISIONS WITH THE AMY DETECTOR

RYOTARO TANAKA*
Chuo University
1-13-27 Kasuga, Bunkyoku, Tokyo 112, Japan

ABSTRACT

We presents results of an experimental study of $e^+e^- \rightarrow e^+e^- + hadrons$ with the no-tag condition. We observe more events than expected from the incoherent sum of QPM and VMD models and give a quantitative explanation of the excess by including the hard scattering effects of the hadronic constituents of the photons calculated with QCD.

Also presented are results of a measurement of the photon structure function F_2^γ at averaged Q^2 =51 $(GeV/c)^2$. The measured structure function is compared with the incoherent sum of the VMD and QCD predictions.

1. Analysis of Untag-Events

We report on an experimental study of the production of high transverse momentum hadrons in high energy $\gamma\gamma$ collisions. The experiment uses reactions of the type $e^+e^- \rightarrow e^+e^- + hadrons$ at $E_{cm} \simeq 60$ GeV, where both the electron and positron scatter at small angles (untagged events) and the virtual photons are nearly on the mass shell. Previous measurements of this process, at lower center-of-mass (c.m.) energies,[1-3] report an excess of events over the sum of the expectations from the Quark-Parton Model (QPM, see Fig. 1a) and the Vector-Meson Dominance Model (VMD, see Fig. 1b). These experiments note that the excess events do not have the two-jet topology that is characteristic of the QPM diagram but provide no quantitative explanation for the effect.

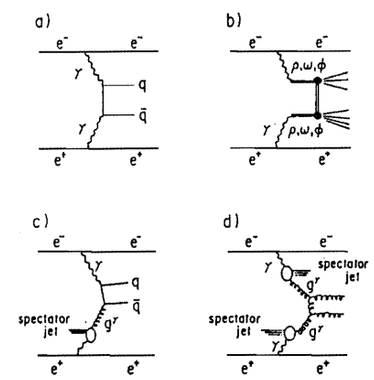

Fig. 1. Diagrams for the a) QPM, b) VMD, and examples of c) 3-jet and d) 4-jet hard-scattering processes used in MJET.

Recent QCD-based calculations show that non-diffractive hard scattering of hadronic constituents of the photons (see Figs. 1c and 1d) produce high transverse momentum (high-p_t) hadrons in multiple-jet configurations.[4,6] The cross section for high-p_t hadron production by these processes increases with energy, becoming comparable to the contributions from QPM and VMD at c.m. energies near 60GeV. The rate for these hard scattering processes is sensitive to the parton content of the photon.

The experiment reported here is based on a 27.5 pb^{-1} data sample accumulated in the AMY detector at the TRISTAN e^+e^-storage ring, at c.m. energies ranging from 55 to 61.4 GeV. We observe an excess that is higher than seen in the earlier experiments and provide, for the first time, a quantitative explanation for the effect in terms of hard scattering of the hadronic constituents of the photons. The early results of the experiment has already been published.[7] Since then we have improved the Monte Carlo calculations of the hard scattering of the hadronic component of the photon by taking into account the effects of the finite mass of the charm quark (in the previous analysis the mass of charm quark was neglected).

1.1. *Event selection*

Untagged hadronic events produced by $\gamma\gamma$ interactions were selected by requiring:

- The number of charged tracks with polar angle in the range $25° \leq \theta \leq 155°$ must be at least 4, and of these at least two must have $|P| > 0.75$ GeV/c and at least one must have $p_t > 1.0$ GeV/c.
- The most energetic cluster appearing in the calorimeter, covering $|\cos\theta| \leq 0.97$, must have an energy less than $0.25E_{beam}$ (anti-tagging).
- The net charge of the observed charged tracks $\sum q_i \leq 2$.
- The net transverse momentum $|\sum \vec{p}_{t,i}|$, where the $\vec{p}_{t,i}$ are the projections of the observed momenta on the plane transverse to the beam, must have magnitude ≤ 2.5GeV/c.
- The mass of the system of observed hadrons must be in the range 4 $GeV/c^2 \leq W_{vis} \leq 15$ GeV/c^2, where the computation of W_{vis} includes both charged and neutral particles and assumes the pion mass for all charged particles.

The 3178 events that survive these cuts were visually scanned by physicists. In the scan, 439 events were attributed to degraded beam particles interacting in the wall of the vacuum chamber and were discarded. Hadronic annihilation events with either initial state radiation or large missing energy satisfy the $e^+e^- \rightarrow e^+e^- + hadrons$ selection criteria. The level of this contamination was estimated using an event sample generated by the Lund 6.3 generator and passed through a detector simulation program. The contamination from $e^+e^- \rightarrow \tau^+\tau^-$ and $e^+e^- \rightarrow e^+e^-\tau^+\tau^-$ was also estimated by using Monte Carlo simulated events for these processes. We obtained the following results:

*Representing the AMY Collaboration

- hadronic annihilation events: 68 ± 4 events;
- $e^+e^- \to e^+e^-\tau^+\tau^-$: 71 ± 4 events;
- $e^+e^- \to \tau^+\tau^-$: negligibly small.

From the distributions of the vertex position along the beam we conclude that the residual contamination from beam-gas events is negligibly small.

The trigger efficiency was estimated using a Monte Carlo simulation for $e^+e^- \to e^+e^- + hadrons$ to be 96.2 ± 1.6%. After all background subtractions and efficiency corrections, we obtain a final count of 2703 ± 98 events.

1.2. *Monte Carlo study*

The experimental data were compared with the predictions of models for high-p_t hadron production in $\gamma\gamma$ reactions using Monte Carlo simulations. Point-like interactions of photons are modeled using a QPM event generator that incorporates all first-order QED radiative corrections. The QPM events are fragmented via the Lund parton-shower scheme with the default parameters. In the previous study the LUND string fragmentation scheme was used for the QPM.[7] A sample of simulated VMD events were produced using the techniques developed by the PLUTO group.[1] The GVDM formula was used for the generation of VMD with the cross section $\sigma_{\gamma\gamma}$=240(nb). The created quark-antiquark system was fragmented via the Field-Feynmann scheme by using PLUTO tuned parameter with the limited-pt distribution given by the formula exp(-5pt^2).

In addition to these processes, hard, non-diffractive hadronic interactions take place between photons when a constituent parton in one of the photons interacts with the other photon or one of its constituents as indicated in Fig.1c and 1d. In these processes, the interacting constituents produce wide-angle jets and the noninteracting constituents produce spectator jets in the directions of the incident virtual photons, which are very near to the directions of the incident beam particles. These events were generated based on the formulae given in ref.[4] Here the parton densities in the photon were taken from two parametrizations, that is, Drees and Grassie (DG),[5] and Levy, Abramowics and Charchula (LAC)[6] parametrizations. According to the simulation results, half of the secondary particles from the spectator jets can be detected within the present angular acceptance. Therefore, events corresponding to the processes indicated in Figs 1c and 1d are expected to appear as events with three and four jets, respectively. So we call them as multi-jet (MJET) events. The MJET cross section for three-(four-) jet events is given by the product of the luminosity functions of two photons, the parton density inside one photon (parton densities inside two photons), the subprocess cross section for the interaction between a parton and a photon (between two partons), and a kinematical factor. The subprocess cross sections have been calculated by the perturbative-QCD.

Both the parton densities of DG and LAC parametrization are obtained by solving the leading-order Q^2 evolution equation. The Q^2 evolution of DG parametrization starts from Q_0^2=1 (GeV/c)^2 and parameters are fitted to explain only the PLUTO single tag data at Q^2 =5.3 (GeV/c)^2 by imposing some relations among singlet quark density, non-singlet quark density and gluon density . LAC parametrizations are obtained by fitting parameters to all the available F_2^γ experimental data from lower Q^2 (1 (GeV/c)^2) to higher Q^2 (100 (GeV/c)^2) without any relationships among parton densities. The three kinds of LAC density functions are available, LAC1,2 and 3. The Q^2 evolution of LAC1,2,3 density starts from Q_0^2 = 4.0, 4.0, 1.0 (GeV/c)^2, respectively. The difference of quark density function between DG and LAC is very small for the higher Q^2 region, however in the small Q^2 region around 1 (GeV/c)^2 we see some difference at larger-x region. Especially, there can be seen the large difference between gluon densities in all Q^2 region. In DG model, the density function of charm quark is assumed to be the same as that of u-quark. The QCD scale parameter Q^2 is chosen to be P_T^2 of the outgoing partons. In our previous analysis,[7] we treated all quarks as massless so that the number of flavor was taken to be 4. In the present analysis we treat charm quark as massive. As a result the number of flavor is taken to be 3 and the cross sections of the subprocesses with charm quark in the final state include the effects of finite mass of charm quark and those with charm quark in the initial state are negligibly small and neglected.

Simulation of MJET processes are carried out by producing two high-P_T partons and one (two) spectator parton(s) for three- (four-) jet events. The spectator jet is simulated by generating a parton in the incident beam direction.* In order to guarantee the applicability of QCD and avoid double counting between the soft (diffractive) and hard (non-diffractive) contributions, we only generate events with parton P_T values larger than a cutoff P_T^{min}. Aside from the fact that the applicability of perturbative QCD requires P_T^{min} to be greater than about 1 GeV/c, the appropriate value for the cutoff is not known. The produced partons are then fragmented via the Lund string-fragmentation scheme with default parameters. The generated particles are identified with one of two back-to-back jets in the c.m. system of the detected hadrons using the thrust axis to define the jet axis. We define P_T^{jet} as the component of the jet momentum transverse to the beam direction.

1.3. *Results*

Various distributions, such as those of P_T^{jet}, W_{vis} , multiplicity, and individual particle p_t, were determined using a bin-by-bin background subtraction and compared with Monte Carlo simulations. The general features of these distributions are found to be well described by the incoherent sum of QPM, VMD and MJET as can be seen in Figs. 2, where in the MJET model we use the DG parton density functions and

*The transverse momentum(P_T) of a spectator jet w.r.t the beam direction is expected to have a finite value less than around a few GeV/c. But the effects of the finite $P_T$value of the spectator jet were found to be quite small.

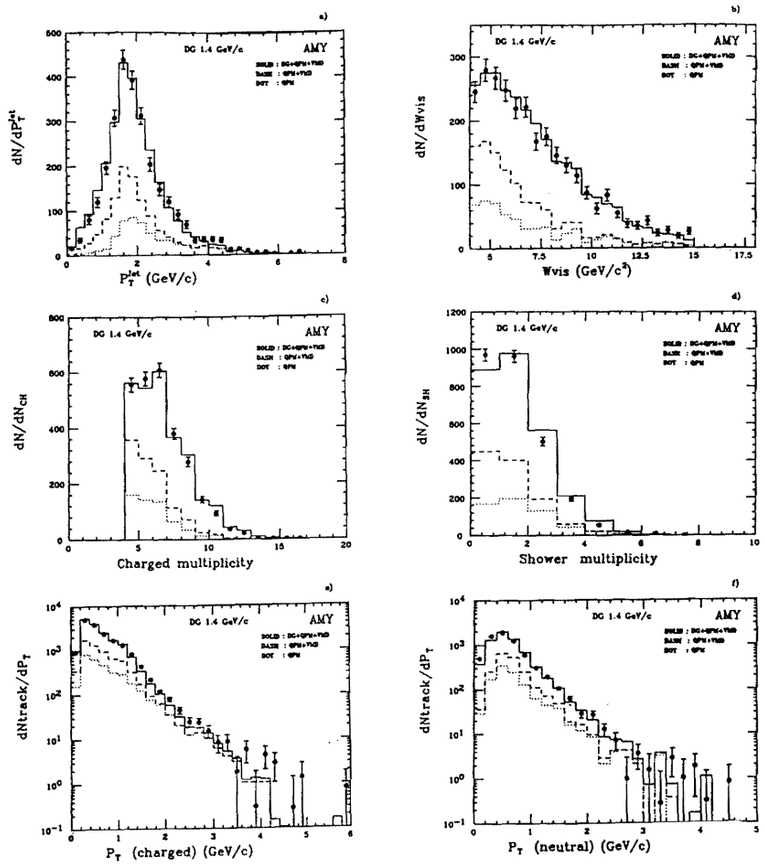

Fig. 2. Comparison of the observed distributions with Monte Carlo simulations. The histograms are the predictions of i) QPM (dotted), ii) QPM + VMD (dashed), and iii) QPM + VMD + MJET (solid) with the DG parton densities and P_T^{min}=1.4 GeV/c. a) P_T^{jet}. b) Invariant mass of observed hadronic particles. c) Charged multiplicity. d) Neutral multiplicity. e) P_T of charged tracks. f) P_T of neutral tracks.

set the cutoff parameter P_T^{min} to 1.4 GeV/c. The MJET prediction is sensitive to the choice of the value of P_T^{min}. The P_T^{min} value is chosen such that the simulated events agree with the P_T^{jet} distribution above 1.5 GeV/c where the MJET contribution

is much larger than the VMD contribution (see Fig. 2a). However, the thrust distribution shows some discrepancy at the thrust values below 0.85 as seen in Fig. 3a. In the previous analysis with massless charm quark the discrepancy in the thrust distribution was observed only at the thrust values between 0.75 and 0.85. So the new MJET calculation gives worse fit to the data than before. It is mainly due to the change of the relative contributions of 3-jet and 4-jet events.

In the low P_T^{jet} region, we would expect a large systematic error due to large uncertainties of measured VMD cross sections in $\sigma(W)$. In order to reduce the error and obtain better comparison with the QCD calculations we selected events with $P_T^{jet} \geq$ 3 GeV/c where VMD contribution is negligibly small. The features of the resulting various distributions except for the thrust distribution are also well described by the incoherent sum of QPM, VMD and MJET with P_T^{min}=1.4 GeV/c. The large excess of events over the QPM prediction at low thrust region is well described by the contribution from the MJET model for the thrust below 0.75 (see Fig. 3b). However, for the thrust values between 0.75 and 0.85 predicted number of events of QPM + MJET is still much below the observed data. When we use P_T^{min}=1.6 GeV/c we have better agreement at lower thrust values(Fig. 4), but the overall agreement is not improved.

We have also compared our data with the predictions obtained by using parton densities for LAC models, LAC1 and LAC3. The density function of LAC1 shows moderate distribution both for quark and gluon densities in the x-space, on the other hand LAC3 shows an abnormally hard gluon density distribution. Here, we set the P_T^{min} = 2.0(3.0) GeV/c for LAC1(LAC3), respectively. The MJET predictions obtained by using the LAC1 density functions are similar to those obtained from the DG density functions and explain the general features of the various observed distributions. For example in Fig. 5, we show thrust distributions. However, the prediction for the LAC3

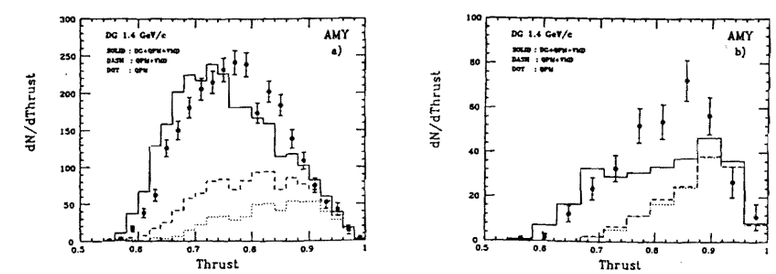

Fig. 3. Comparison of the observed thrust distribution with Monte Carlo simulations. The histograms are the predictions of i) QPM (dotted), ii) QPM + VMD (dashed), and iii) QPM + VMD + MJET (solid) with the DG parton densities and P_T^{min}=1.4 GeV/c. a) Thrust for all events. b) Thrust for the events with P_T^{jet} above 3 GeV/c.

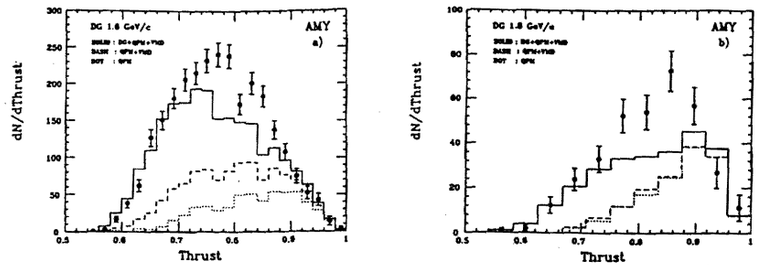

Fig. 4. Comparison of the observed thrust distribution with Monte Carlo simulations. The histograms are the predictions of i) QPM (dotted), ii) QPM + VMD (dashed), and iii) QPM + VMD + MJET (solid) with the DG parton densities and P_T^{min}=1.6 GeV/c. a) Thrust for all events. b) Thrust for the events with P_T^{jet} above 3 GeV/c.

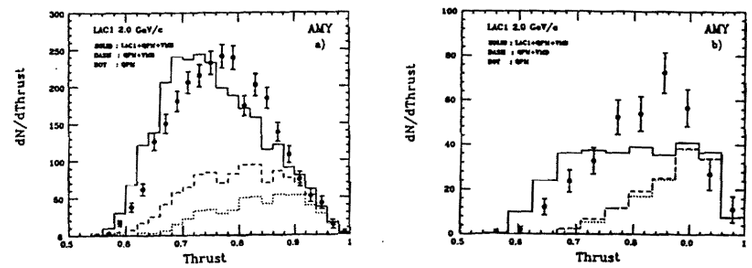

Fig. 5. Comparison of the observed thrust distribution with Monte Carlo simulations. The histograms are the predictions of i) QPM (dotted), ii) QPM + VMD (dashed), and iii) QPM + VMD + MJET (solid) with the LAC1 parton densities and P_T^{min}=2.0 GeV/c. a) Thrust for all events. b) Thrust for the events with P_T^{jet} above 3 GeV/c.

disagree with the data. For example, we show P_T^{jet} and W_{vis} distributions for all events, thrust and W_{vis} distributions for events with $P_T^{jet} \geq$ 3.0 GeV/c in Fig. 6. We can not obtain the better agreement by tuning P_T^{min}. This reflects the abnormally hard gluon density function of the LAC3. Therefore we can exclude the possibility of the LAC3 parametrization for the parton density of the photon. The discrepancy observed in the thrust distribution for the DG model is also existing for the LAC1 model. The lack of predicted events at medium thrust region seems to indicate existence of some events which have the feature like the mixture of two-jet and three-jet topology. One possibility to explain this feature could be the use of the new density function with harder

quark density and relatively softer gluon density. An example of the parton densities with such featues was obtained by Gordon and Storrow.[8] This study is planed to be pursued soon. Tuning of the fragmentation parameter σ_q of Lund string fragmentation was found to fail to improve the discrepancy of the thrust distribution.

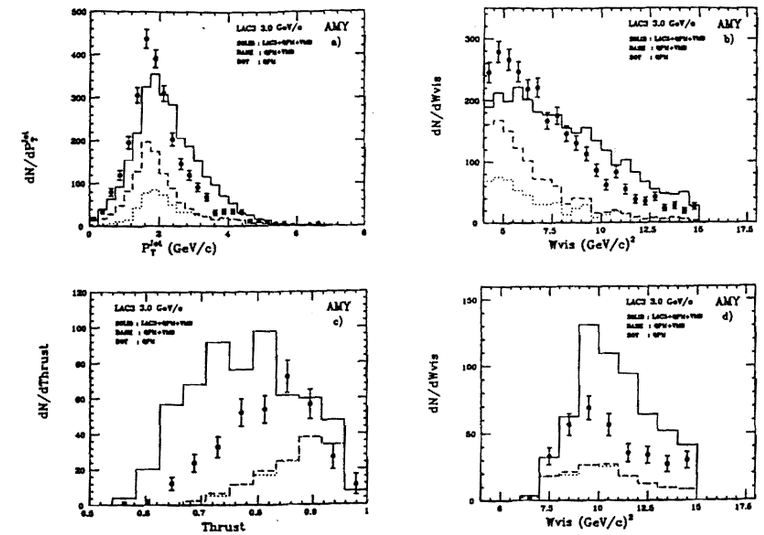

Fig. 6. Comparison of the observed distributions with Monte Carlo simulations. The histograms are the predictions of i) QPM (dotted), ii) QPM + VMD (dashed), and iii) QPM + VMD + MJET (solid) with the LAC3 parton densities and P_T^{min}=3.0 GeV/c. a) P_T^{jet} . b) Invariant mass of observed hadronic particles. c) Thrust for the events with P_T^{jet} above 3 GeV/c. d) Invariant mass of observed hadronic particles for the events with P_T^{jet} above 3 GeV/c.

2. Analysis of Single-tag Events

Hadron production in $\gamma\gamma$ collisions between virtual photon and quasi-real photon can be studied in reactions of the type $e^+e^- \rightarrow e^+e^-$+hadrons where one of the final-state electrons is observed at large angles relative to its incident direction while the other electron remains at small angles and is unobserved (the single-tag condition). This process can be interpreted as the deep inelastic scattering of an electron from an almost real photon so that its cross section can be expressed in terms of the photon structure function F_2^γ.

Measurements by PEP and PETRA experiments for Q^2 values ranging from a

few $(GeV/c)^2$ to 100 $(GeV/c)^2$ have shown that the cross section is dominated by the contribution to F_2^γ from the point-like photon-quark coupling for Q^2 values larger than 20 $(GeV/c)^2$.[9–11] Since at high values of Q^2 both QPM and perturbative QCD calculations[12,13] of F_2^γ are expected to be valid, measurements in this region test the validity of these models.

We have already published the results of a measurement of the photon structure function F_2^γ at three average Q^2 values of 73, 160 and 390 $(GeV/c)^2$ which were obtained using the early data of the AMY detector.[14] In the previous analysis we used the endcap shower counters consisting of the pole tip counter (PTC) and the ring shower counter (RSC) and the barrel shower counter (SHC) for the tagging device. We report here a new measurement of F_2^γ at average Q^2 value of $51(GeV/c)^2$ using the new end cap shower counter (ESC) as the tagging device. The endcap region of the AMY detector has been upgraded to obtain better angular acceptance and better granularity in the forward region by removing the PTC as well as the RSC and installing the ESC. The ESC detector which has angular coverage between 11° and 37° with total $15X_o$ thickness is consisting of the lead/scintillator sandwitched EM-shower counter being interspersed by the position-sensitive gas chamber. The position of shower cluster is measured with the resolution $\Delta\theta$=4 mrad, $\Delta\phi$= 14 mrad and the energy resolution is given by $\Delta E/E = 29\%/\sqrt{E} + 6\%$. A 27.2 pb^{-1} data sample accumulated at the center-of-mass energy of 58 GeV was used for the present analysis.

2.1. *Event selection*

The ESC tagged events were selected using the following criteria:

- A cluster with an energy exceeding $0.5E_{beam}$ is observed in the ESC in the angular range $12° \leq \theta_{tag} \leq 25°$.
- No additional clusters with energies exceeding $0.25E_{beam}$ are observed anywhere in the barrel and endcap shower counters (anti-tagging).
- The charged multiplicity is three or more, with no tagged electron candidates in the CDC. Charged tracks are required to have at least 9 axial and 6 stereo hits, polar angles in the range $|\cos\theta| \leq 0.91$, and originate from within $\Delta R \leq 2.5$ cm and $\Delta Z \leq 7.5$ cm of the interaction point.
- The observed mass of the hadron system, W_{vis} , is required to be $W_{vis} \geq 1.0$ GeV/c^2, where W_{vis} is calculated by assuming pion masses for all charged particles. Only those shower clusters in the SHC (ESC) with energies larger than 0.4 GeV (0.5 GeV) were included in the W_{vis} calculation.
- The total visible energy of the hadron system is $E_{vis} \leq 0.4\sqrt{s}$.
- The normalized longitudinal momentum imbalance (NLMB) is greater than 0.1, where NLMB= $(\cos\Theta_{tag}/|\cos\Theta_{tag}|)\sum p_i\cos\theta_i/E_{beam}$, with the sum taken over all charged and neutral particles in the event (including the tagged electron) and Θ_{tag} is the polar angle of the tagged electron.
- The normalized transverse momentum imbalance (NTMB) is less than 0.5 GeV/c, where NTMB= $|\sum p_{t,i}|/E_{beam}$, with $p_{t,i}$ being the momentum vector of any particle (including the tagged electron) in the plane perpendicular to the beam direction.

The 206 events that survive these cuts were subjected to a visual scan where 4 events were rejected as the background. The remaining 202 events were corrected for backgrounds, estimated using Monte Carlo simulations, as follows:

- $e^+e^- \to e^+e^-\tau^+\tau^-$: 19.1 events;
- multihadronic single-photon annihilation events: 19.1 events;
- inelastic Compton scattering: 4.0 events;
- $e^+e^- \to \tau^+\tau^-$: negligibly small.

The background from beam interactions in the residual gas of the vacuum chamber was estimated from the data. The event rate for detected events that had vertices upstream and downstream of the interaction point was found to be negligibly small. After subtracting background events a 165.5 ± 14 event signal remains. The Q^2 values of these events range from 15 to 150 $(GeV/c)^2$ with the average being 51 $(GeV/c)^2$.

2.2. *Monte Carlo Simulation*

The QCD calculation of F_2^γ by Field *et al.*[12] has shown that the hadronic part and the point-like part of F_2^γ can separately be made free from the singularities that occur near x=0 by the introduction of a single phenomenological parameter, which can be taken to be either t_0 or p_t^0, the value of t or p_t at the boundary between the hadronic and point-like regions of phase space. Here t is the square of the four-momentum transfer of the virtual quark at the target-photon vertex plus the the quark mass squared, and p_t is the transverse momentum of the outgoing quark with respect to the target photon. Recently, Kapusta has calculated the QCD structure function in x space up to all orders of α_s.[13] For the heavy quarks (c and b) we use the QPM expression for F_2^γ which takes into account the effects of heavy quark mass. In addition, we neglect the influence of t_0 and p_t^0 on the expression, assuming that the value of p_t^0 is smaller than the heavy quark masses. For the hadronic part of F_2^γ that is not calculable by perturbative QCD, we use the VMD estimate derived from measurements of TPC/2γ group.[15]

We compare our experimental results with the predictions of the sum of the all-order QCD predictions with Λ = 0.2 GeV for the light quarks (u,d,s), the QPM prediction for heavy flavors (c,b), and the hadronic contribution of VMD.

The produced quarks are fragmented into hadrons using the Lund string fragmentation scheme with default parameters. The quark masses are taken to be: $m_u = m_d = 325$ MeV/c^2, $m_s = 500$ MeV/c^2, $m_c = 1.6$ GeV/c^2 , and $m_b = 5$ GeV/c^2. The generated events are then processed through a detector simulation program and subjected to the same analysis program that is used for the real data.

2.3. Results

Various distributions, such as those of the charged and neutral multiplicities, the charged and neutral P_T w.r.t. the beam axis, the energy and angle of the tagged electrons, W_{vis} , Q^2 , and x_{vis}, where $x_{vis} = Q^2/(Q^2 + W_{vis})$, calculated using a bin-by-bin background subtraction, are found to be well reproduced by Monte Carlo simulations based on QCD(uds)+QPM(cb)+VMD for p_t^0 =0.5 GeV/c. In order to facilitate the comparison of the data with theory, we have extracted the photon structure function F_2^γ by using the unfolding procedure described in ref.[11] The unfolded F_2^γ functions are shown in Fig. 7 and they include the statistical errors only. Also included in the figure are the theoretical predictions for F_2^γ at $Q^2 = 51$ (GeV/c)^2 for various values of t_0 (Fig. 7(a)) and p_t^0 (Fig. 7(b)). These are calculated by summing the QCD prediction for the light quarks with $\Lambda = 0.2$ GeV, the QPM prediction for the heavy quarks, and the VMD contribution for the hadronic part. The data are consistent with the QCD predictions if t_0 is taken to be below 2 (GeV/c)^2 or p_t^0 below 1 GeV/c. In Fig. 8(a)-(b) we compare the measured F_2^γ with the QCD predictions of the DG and LAC1 models which are obatined by solving the QCD evolution equations using the other experimental data of F_2^γ. As seen in the figures, the prediction of DG and LAC1 agree well

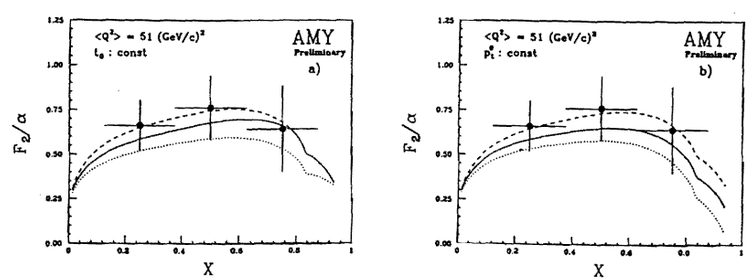

Fig. 7. Comparison of the x dependence of the photon structure function F_2^γ at an average $Q^2 = 51$ (GeV/c)^2. Circles are the data points with error bars which include only statistical errors. The curves are the sum of the all-order QCD predictions with $\Lambda = 0.2$ GeV for the light quarks (u,d,s), the QPM prediction for heavy flavors (c,b), and the hadronic contribution given by VMD. The QCD predictions are calculated for $t_0 = 0.1$(dashed), 0.5(solid)and2.0(dotted)(GeV/c)^2. b) The QCD predictions are calculated for $p_t^0 = 0.1$(dashed), 0.5(solid)and1.0(dotted)GeV/c.

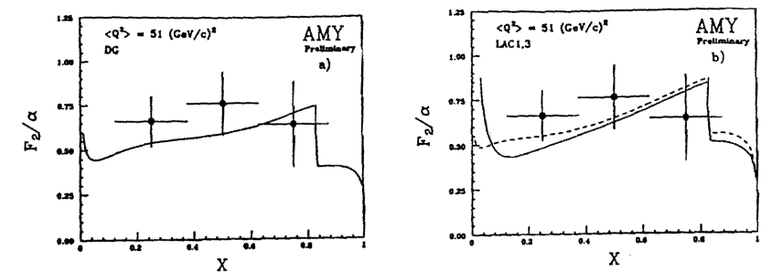

Fig. 8. Comparison of the x dependence of the photon structure function F_2^γ at an average $Q^2 = 51$ (GeV/c)^2. The curves are the fitted QCD predictions of a) DG parametrization, b) LAC1 (solid) and LAC3 (dashed) parametrizations.

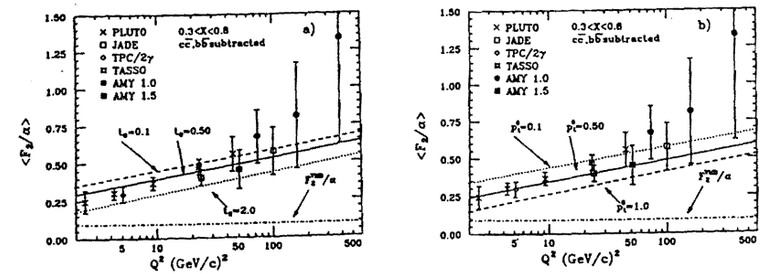

Fig. 9. The Q^2 evolution of F_2^γ averaged over the intermediate x region between 0.3 and 0.8. QPM estimates for the contributions from the heavy flavors (c,b) are subtracted from the data. The curves are the sum of the predictions of QCD, with $\Lambda = 0.2$ GeV, and VMD. a) QCD calculations for $t_0 = 0.1, 0.5$ and 2.0 (GeV/c)^2. b) QCD calculations for $p_t^0 = 0.1, 0.5$ and 1.0 GeV/c.

with our data within statistical errors.

A basic feature of QCD is the Q^2 evolution of the structure function. In Figs. 9-10 we show the average values of observed F_2/α for the light quarks in the intermediate x region between 0.3 and 0.8, where we have included the VMD contribution, together with previously reported measurements from other experiments over the Q^2 range from a few (GeV/c)^2 to 100 (GeV/c)^2. The sums of the QCD predictions and the VMD prediction are also plotted in the Fig. 9. The QCD predictions are calculated using $\Lambda = 0.2$ GeV for various t_0 (Fig. 9(a)) and p_t^0 values (Fig. 9(b)). Our experimental data

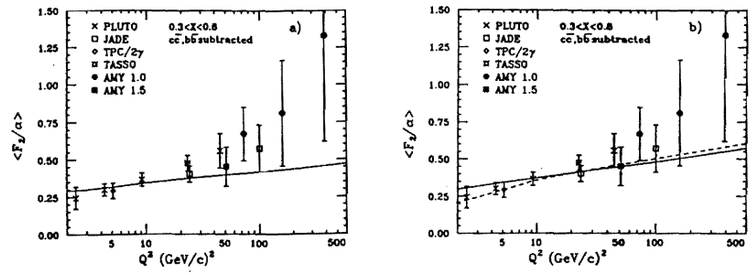

Figs.10 The Q^2 evolution of F_2^γ averaged over the intermediate x region between 0.3 and 0.8. QPM estimates for the contributions from the heavy flavors (c,b) are subtracted from the data. The curves are the fitted QCD predictions of a) DG parametrization, b) LAC1 (solid) and LAC3 (dashed) parametrizations.

are consistent with the QCD prediction if the value of t_0 (p_t^0) is taken to be below 2 $(GeV/c)^2$ (1 GeV/c). The predictions corresponding to DG and LAC1 models are also shown in Figs. 10. Our data again consistent with DG and LAC parametrizations within statistical errors.

References

1. Ch. Berger *et al.*(PLUTO), *Z. Phys.* **C33** (1987) 351.
2. H.-J. Behrend *et al.*(CELLO), *Z. Phys.* **C51** (1991) 365.
3. H. Aihara *et al.*(TPC/2γ), *Phys. Rev.* **D41** (1990) 2667.
4. M. Drees and R.M. Godbole, *Nucl. Phys.* **B339** (1990) 355.
5. M. Drees and K. Grassie, *Z. Phys.* **C28** (1985) 451.
6. A. Levy, H. Abramowics, and K. Charchula, *Phys. Lett.* **B269** (1991) 458.
7. R. Tanaka *et al.*(AMY), *Phys. Lett.* **B277** (1992) 215.
8. L.E. Gordon and J.K. Storrow, *Manchester preprint M/C.TH.91/29.*
9. Ch. Berger *et al.*(PLUTO), *Phys. Lett.* **B107** (1981) 168 , ibid **B142** (1984) 111; H.J.Behrend *et al.*(CELLO), *Phys. Lett.* **B126** (1983) 391; A. Aihara *et al.*(TPC/2γ), *Phys. Rev. Lett.* **58** (1987) 97; *Z. Phys.* **C34** (1987) 1; M. Althoff *et al.*(TASSO), *Z. Phys.* **C31** (1986) 527.
10. Ch. Berger *et al.*(PLUTO), *Nucl. Phys.* **B281** (1987) 365.
11. W. Bartel *et al.*(JADE), *Z. Phys.* **C24** (1984) 231.
12. J.H. Field, F. Kapusta and L. Poggioli, *Phys. Lett.* **B181** (1986) 362; ibid *Z. Phys.* **C36** (1987) 121.
13. F. Kapusta, *Z. Phys.* **C42** (1989) 225.
14. T. Sasaki *et al.*(AMY), *Phys. Lett.* **B252** (1990) 491.
15. R.R. McNeil, Ph.D. thesis, UC Davis report (1986) (unpublished).